Neutron activation measurements on natural tellurium

R. Reifarth* and F. Käppeler†
Forschungszentrum Karlsruhe, Institut für Kernphysik, Postfach 3640, D-76021 Karlsruhe, Germany
(Received 8 May 2002; published 27 November 2002)

Natural tellurium has been activated with thermal neutrons ($kT=22$ meV) and with quasistellar neutrons ($kT=25$ keV). By analyzing the ground state decay of the odd isotopes as a function of time, information on the partial capture cross sections to the isomeric states could be determined with systematic uncertainties of 3–8 %. Additionally, the decay parameters of some isomers could be significantly improved. These results are of relevance for *s*-process nucleosynthesis.

DOI: 10.1103/PhysRevC.66.054605 PACS number(s): 25.40.Lw, 25.70.Gh, 27.60.+j, 97.10.Cv

I. INTRODUCTION

Neutron capture on the even tellurium isotopes populates either the ground states or the isomers of the odd reaction products, which are located around 100-keV excitation energy. For thermal neutrons (22 meV) the partial capture cross section to the isomer is about ten times smaller than the cross section to the ground state. This large difference complicates a reliable experimental determination of their ratio, which is interesting from the astrophysical point of view.

At the high temperatures during He burning in asymptotic giant branch (AGB) stars, where neutron capture nucleosynthesis of the slow process (*s* process) takes place, the depopulation of isomeric states can be dramatically accelerated. The mechanism for this enhancement is provided by the energetic thermal photon bath which can populate excited nuclear states up to 1 MeV. Starting from an isomer, it may well be possible to reach levels with a non-neglible decay branch to the ground state. If the ground state has a short half-life—like all the unstable odd Te nuclei under consideration—the isomer can be efficiently destroyed before it can capture a neutron, and has therefore no consequence for the reaction flow. However, if the isomer is not destroyed, it may act as a branching point in the reaction path, as discussed below. Whether such mediating states can be reached depends on their excitation energies as well as on the prevailing temperature.

Present stellar models [1,2] are describing the *s* process in the Te-I-Xe region to occur by alternative neutron production at temperatures of $T_8=1$ and $T_8=3$ (units of 10^8 K), corresponding to thermal energies of 8 and 25 keV, respectively. Depending on the position of the lowest mediating state, this may imply for some isotopes that ground state and isomer are not in thermal equilibrium, at least at the lower temperature. Therefore the partial stellar (n,γ) cross sections of ^{126,128}Te have been studied for a complete description of the interesting branching at ^{128}I.

As shown in Fig. 1 the *s*-process reaction flow between Te and Xe is characterized by a sequence of neutron captures on the stable isotopes. At the unstable isotope ^{127}Te, however, a small branching of the path may result from the competition between the dominant β decay and possible neutron captures on the 109-d isomer. A branching of different nature occurs at ^{128}I where the competition is between the β^- and electron capture (EC) decays. The combined strength of these branchings is defined by the abundances of the *s*-only isotopes ^{128}Xe and ^{130}Xe, since the first one is partially bypassed by the reaction flow. The $A=128$ branching is appealing since the half-life of ^{128}I is far too short for neutron captures, thus being an indicator for the temperature- and density-dependent interplay between its weak interaction rates, completely independent of the stellar neutron flux. In this context, the branching at ^{127}Te constitutes a necessary correction. The half-life indicated in Fig. 1 was derived under the assumption that the population of ground state and isomer are completely determined by the equilibrium between excitation via thermal photons and the corresponding decays [3]. This potential correction for the branching at ^{127}Te motivated the measurements at thermal and stellar energies described in Sec. II. The respective data analyses and

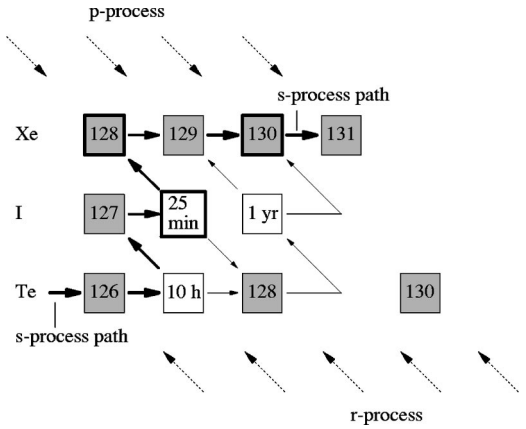

FIG. 1. The *s*-process reaction path between Te and Xe. In contrast to ^{130}Xe, ^{128}Xe is partly bypassed due to the interesting temperature dependent branching at ^{128}I and the possibly small branching at ^{127}Te. Both Xe isotopes are shielded against *r*-process contributions by their stable Te isobars. If it would be possible to neglect the branching at ^{127}Te, one could draw conclusions about the temperature during the *s* process, since the branching at ^{128}I results from the competition between β^- and electron capture decays and is completely independent of the neutron flux. The indicated half-life of ^{127}Te corresponds to complete thermal equilibration of ground state and isomer (see text).

*Electronic address: rene.reifarth@ik.fzk.de
†Electronic address: franz.kaeppeler@ik.fzk.de

results are presented in Secs. III and IV, followed by a brief outline of the astrophysical impact in Sec. V.

II. EXPERIMENT

If neutron capture produces an unstable isotope the activation technique provides a powerful tool for cross section measurements. This technique offers a twofold advantage: (i) It does not require isotopically enriched samples since the capture reactions can be identified via γ spectroscopy of transitions in the decay of the product nuclei. (ii) It allows us to achieve very good sensitivity since the irradiation can be performed in high neutron fluxes and since comparably high detection efficiencies can be obtained with large HPGe detectors.

A. Sample preparation

The samples were pressed from natural tellurium powder. For better stability a 1:1 mixture of tellurium and carbon powder was used for producing sample disks of 6 mm in diameter at a pressure of 1 GPa. The samples were mounted between Kapton foils, which were stretched over thin aluminum frames. By using a special tool for centering the samples with respect to the aluminum frames, the sample position was reproducible within 0.1 mm during the activation at the Van de Graaff accelerator as well as during the activity measurement.

B. Activation with thermal neutrons

An activation with thermal neutrons were carried out in order to determine the stellar cross sections in the keV region relative to the well known thermal cross sections. In using the same samples and detection techniques, many systematic uncertainties can be avoided or significantly reduced. In the context of stellar nucleosynthesis it is important to investigate the partial capture cross sections of ^{126}Te and ^{128}Te, since the respective isomers may act as branching points in the reaction flow. Moreover, even at thermal energies the isomeric ratios

$$IR = \frac{\text{partial capture cross section to isomer}}{\text{total capture cross section}}$$

of some Te isotopes exhibit significant discrepancies which are important to resolve [4,5].

The activation was carried out at the TRIGA-HD II reactor of the German Cancer Research Center, Heidelberg. The flux at the internal irradiation position used was $\Phi_{th} = 10^{11}$ cm^{-2} s^{-1} with an epithermal component of 5%. The number of activated nuclei ^{A+1}N can be expressed in terms of the thermal cross section σ_{th}, the resonance integral I_{res}, and the ratio between epithermal and thermal neutron flux ρ,

$$^{A+1}N = {}^{A}N \cdot (\Phi_{th}\sigma_{th} + \Phi_{epi} I_{res}) = {}^{A}N \cdot \Phi_{th}\sigma_{th}\left(1 + \rho\frac{I_{res}}{\sigma_{th}}\right),$$

where ^{A}N is the number of atoms in the sample.

TABLE I. Monitor data for the activation with thermal neutrons (Ref. [6]).

Isotope	Weight (mg)	σ_{th} (barn)	Uncertainty (%)	I_{res} (barn)	Uncertainty (%)
^{45}Sc	1.69	27.2	0.74	12	4.2
^{59}Co	0.0286	37.18	0.16	74	2.7
^{197}Au	0.103	98.65	0.09	1550	1.8

The epithermal as well as the thermal flux during the activation can be measured by using different neutron monitors with different ratios I_{res}/σ_{th}. In order to characterize the situation at the TRIGA-HD II reactor, Sc, Co, and Au foils were chosen for this purpose (Table I). Assuming constant neutron flux, the number of activated nuclei is

$$^{A+1}N(t_a, t_w) = {}^{A+1}N\frac{1 - e^{-\lambda t_a}}{\lambda t_a} e^{-\lambda t_w},$$

where λ is the decay constant of the produced isotope, t_a the activation time, and t_w the waiting period between activation and the start of the activity measurement.

The induced activities were measured with a 40-cm^3 coaxial high purity germanium detector (ORTEC). In the beginning the spectra were stored in intervals of 20 min to record the decay of the shorter-lived isotopes, but later on the intervals were extended to 2 h. Even with the small γ intensities of the odd tellurium isotopes, the activities produced at the reactor were high enough to detect the decays of long- and short-lived isotopes with the same detector, keeping the systematic uncertainties small.

The detection efficiency was calibrated with a set of well defined γ sources. Above 120 keV, the measured data points could be represented by a fit according to

$$\epsilon(E_\gamma) = 7.0 \cdot E_\gamma^{-1.3}.$$

Figure 2 shows the excellent agreement between this fit and the calibration measurements over the entire energy range from 120 to 2000 keV.

C. Activation with stellar neutrons

The measurements at keV neutron energies were carried out at the Karlsruhe 3.7 MV Van de Graaff accelerator using the ^{7}Li$(p,n)^7$Be reaction for neutron production. Before each run, the accelerator was operated in pulsed mode with a repetition rate of 1 MHz and a pulse width of 10 ns. This allowed to define the neutron spectra via time of flight (TOF) by means of a ^{6}Li glass monitor located 1 m downstream of the neutron target. For the activations, the accelerator was switched to direct current mode for achieving beam currents around 100 μA. In this mode, the ^{6}Li glass monitor was used for recording the neutron yield in regular intervals of 10 min. The resulting time history was used for evaluating the proper corrections for the decays during activation, f_b [7].

A quasistellar distribution corresponding to a thermal energy of $kT = 25$ keV, which is representative of typical He-

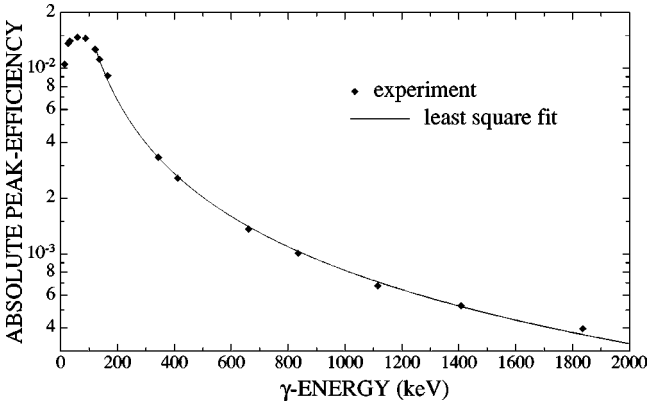

FIG. 2. The detection efficiency versus γ-ray energy of the germanium detector used for the activity measurements after the reactor activations as well as for counting the gold foils used during the activation with stellar neutrons. The solid line shows the least square fit for energies above 120 keV, used for interpolation between the data points.

burning sites, was used in these activations. The spectrum was obtained by bombarding thick metallic lithium targets with a proton beam of $E_p = 1912$ keV, just above the neutron production threshold at 1881 keV. With this choice, all neutrons are emitted in a forward cone of 120° opening angle. The angle-integrated spectrum provides a good approximation of the thermal case, but is truncated at 106 keV [7,8] as illustrated in Fig. 3. The proper proton energy is verified via the 106 keV cutoff in the TOF run with the ^{6}Li glass monitor. The samples were sandwiched between 25-μm-thick gold foils determining the neutron exposure, since both the stellar neutron capture cross section of ^{197}Au [8] and the parameters of the ^{198}Au decay [9] are accurately known. Two activations with different irradiation times were carried out to account for the different half-lives of the produced isotopes.

Compared to the activations with thermal neutrons, both the neutron flux and the cross sections were considerably smaller in the keV region. In order to detect the correspondingly smaller induced activities, an efficient counting system was used in these cases, which consisted of two Clover type HPGe detectors facing each other in close geometry. The Clover detectors (Eurisys Mesures) are an assembly of four independent *n*-type Ge crystals in a four-leaf clover arrangement with 0.2-mm gaps in between. The originally cylindrical crystals with 50-mm diameter and 70-mm length are shaped as shown in Fig. 4, leaving an active volume of about 145 cm^3 per crystal. The crystals are held from the rear through a steel rod of 1-mm diameter and about 35-mm length and are enclosed in a cryostat with a 1-mm-thick aluminum window 5-mm in front.

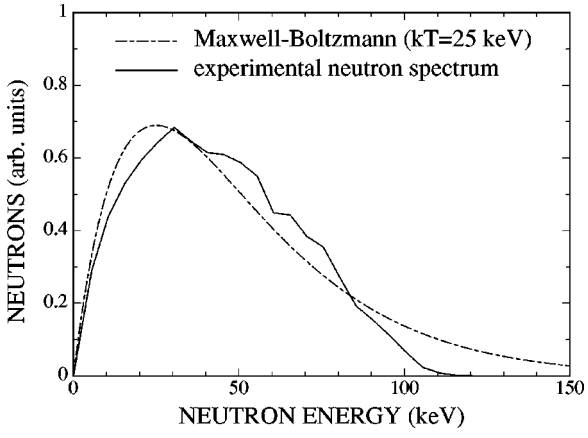

FIG. 3. The neutron spectrum used for the activations at the Van de Graaff accelerator. The experimental spectrum given by the histogram represents a good approximation of a thermal spectrum for $kT = 25$ keV (solid line).

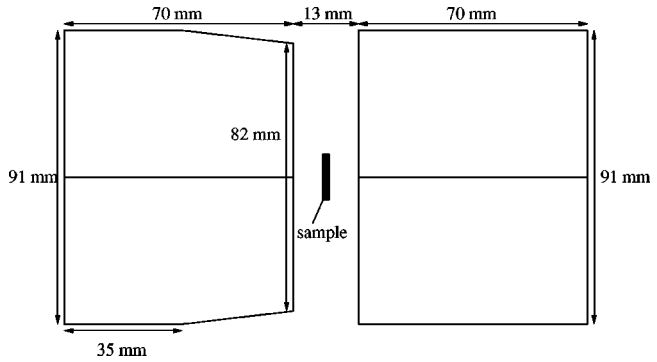

FIG. 4. Arrangement of the Ge crystals and the sample in the face-to-face arrangement of the two Clover detectors used for counting the weak activities obtained with keV neutrons.

The individual Ge crystals have a resolution of typically 2.0 keV at 1.33 MeV. At 122 keV, the peak-to-Compton ratio is ≈ 45. The detector can be operated either in *single mode* by considering the signals from each crystal independently or in *calorimetric mode*, when coincident signals from different crystals are added off-line. In this way Compton-scattered events can be restored in the sum spectrum if the scattered photon is detected in one of the neighboring crystals, resulting in a significantly higher photopeak efficiency.

The detector signals were recorded on PC using the data acquisition system MPA-WIN (FAST Comtec). The respective energy signals were processed in the usual way by spectroscopy amplifiers and analog-to-digital converters (ADC) with fixed conversion times of 800 ns. The data were stored event by event for off-line analysis. A threshold level of 20 keV was set for each ADC.

In view of the low count rates expected for the activation of the isomeric states with very low γ intensities, the two Clover detectors were arranged face-to-face with a distance of only 3-mm, which corresponds to 13-mm distance of the crystals themselves. The sample was exactly centered in the gap by means of a special holder. For this very close geometry the total and peak efficiencies of the Clover system were determined in the range from 50 to 1200 keV using a set of calibrated sources. Measurements were performed at 59 keV (^{241}Am), 88 keV (^{109}Cd), 662 keV (^{137}Cs), 835 keV (^{54}Mn), and 1115 keV (^{65}Zn). For the last two sources, the cascade-summation effect with x rays had to be considered and was calculated with the code CASC [10]. Typical uncertainties of the measured efficiencies are 2% including all statistical and systematic effects.

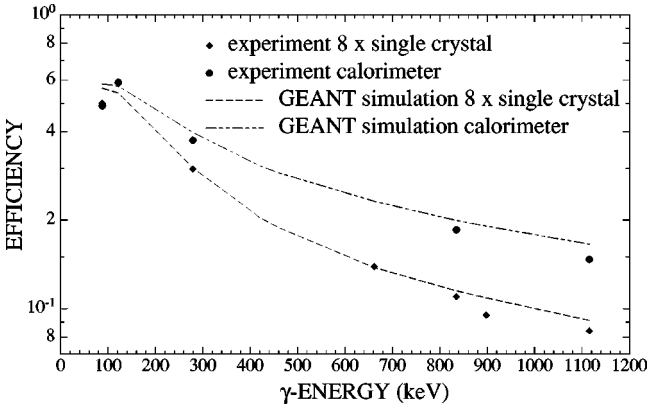

FIG. 5. The photopeak efficiency for the Clover system. The lower data points refer to single crystals, the upper to calorimetric spectra. Experimental data are given by solid symbols, GEANT calculations by dotted lines.

The measurements were supplemented by a Monte Carlo analysis made with the GEANT code [11]. The geometry of the system, including the source holder, was carefully simulated in the calculations. The resulting efficiency for a single crystal is plotted in Fig. 5. The lower curves correspond to the average photopeak efficiency and the upper curves show the calorimeter mode efficiency when coincident events in the other seven crystals are considered. The efficiencies of the individual crystals do not differ by more than $\pm 1\%$. The advantage of the calorimeter mode for the detection efficiency is evident: the ratio of the photopeak efficiency in calorimeter mode and for a single crystal, $\epsilon_{cal}(E)/\Sigma\epsilon_i(E)$, increases from ≈ 1 at 50 keV (where most Compton scattered photons fall below the detection threshold), to ≈ 2 near 1.5 MeV. Above 100 keV the results obtained in the GEANT calculations (solid lines) differ by only a few percent from the experimental values. Therefore the cross section analysis was completely based on lines above 100 keV.

III. ANALYSIS OF THE REACTOR ACTIVATION

A. Determination of the neutron flux

The neutron monitor foils used during the irradiation consisted of 25-μm scandium, 10-μm cobalt, and 0.25-μm gold. All foils were thin enough that neutron self-absorption and absorption losses during γ counting were negligibly small.

For ^{59}Co, the correction for cascade summing could directly be measured by means of a calibrated source, while the 1% correction for ^{45}Sc was determined as described elsewhere [12]. Since the uncertainties of detector efficiency and pile-up corrections were also small, the different resonance integrals of the three monitors allowed us to deduce the flux ratio. A best fit based on the three monitors led to a flux ratio of $(5.5\pm 0.5)\%$. The total neutron flux is not needed in the following analysis.

B. Induced activities

In order to keep the systematic uncertainties as small as possible, the neutron capture cross sections feeding the isomeric states were determined via the activity of the *ground* state decay as a function of time, hence the same γ lines as the capture cross sections to the ground states. This has the advantage that all the uncertainties related to detection efficiency, γ-ray and neutron self-absorption in the sample, cascade corrections, and line intensities cancel out in the relative measurement of the cross section ratios. The only remaining systematic uncertainties are due to the time correlated effects discussed below. The details of the data analysis will be discussed in the next section.

The decay of all investigated isomeric states proceeds partially via the ground state. The time dependence of the ground state abundance is given by

$$\frac{dN^g}{dt}(t) = -\lambda^g \cdot N^g(t) + \eta_i \cdot \lambda^m \cdot N^m(t),$$

where $\lambda^{g,m}$ are the decay constants of ground state and isomer, and η_i the part of internal decays feeding the ground state. While the solution for the isomeric state is given by the decay law $N^m(t) = N^m(0)\exp(-\lambda^m t)$, the solution for the ground state is

$$N^g(t) = N^g(0)\cdot e^{-\lambda^g t} + \frac{\lambda^m}{\lambda^g - \lambda^m}\eta_i \cdot N^m(0)(e^{-\lambda^m t} - e^{-\lambda^g t}).$$

This means that the time dependence of the number of ground state nuclei, and via $A(t) = \lambda N(t)$ the activity of the ground state decay, is a sum of two exponential terms. Since the half-lives of the considered ground states are much shorter than the half-lives of the isomeric states ($\lambda^g \gg \lambda^m$), the activity after irradiation is first determined by the ground state ($\propto e^{-\lambda^g t}$), while the isomer decay dominates at much later times ($\propto e^{-\lambda^m t}$). The analysis of *both* exponential functions was only possible for ^{127,129,131}Te since the ground states of ^{123,125}Te are metastable or stable, respectively. The relevant part of the decay schemes are shown in Figs. 6 and 7, and the corresponding decay data adopted in the analysis are summarized in Table II.

For the three isotopes ^{127,129,131}Te the half-lives of ground and isomeric states are sufficiently different that the approximation $A^g(t) = \lambda^g \cdot N^g(0)\cdot e^{-\lambda^g t}$ can be used immediately after the activation while at later times the activity is due to the decay of the isomer

$$A^g(t) = A^m(t) = \frac{\lambda^g \lambda^m}{\lambda^g - \lambda^m} f_i \cdot N^m(0)\cdot e^{-\lambda^m t}.$$

In these cases it is not necessary to fit two exponentials, one fit for early and later times would be sufficient (Fig. 8).

C. Results and uncertainties

Since the measurements discussed above aimed at the determination of cross section *ratios*, many uncertainties related to the experimental setup cancel in the analysis. According to the previous section, one finds for the number of

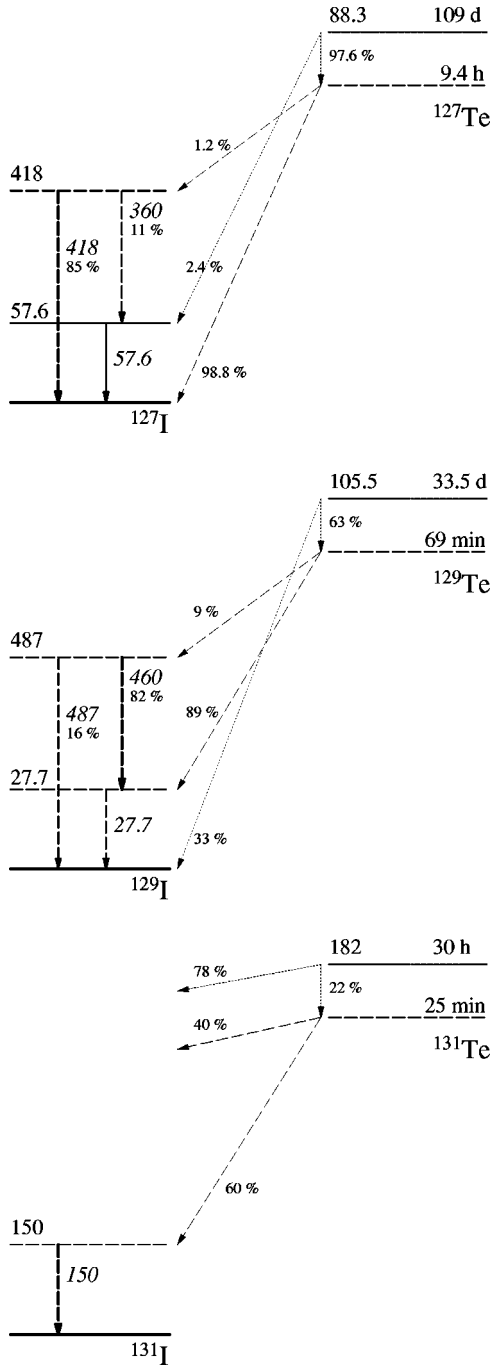

FIG. 6. Simplified decay schemes of those cases where the decays of ground state and isomer could be investigated. All energies are given in units of keV. The transitions used for analysis are indicated by thick arrows.

detector events caused by the ground state decays of the produced Te isotopes as a function of time:

$$C^g(t) = a e^{-\lambda^g t} + b e^{-\lambda^m t},$$

where

$$a := \left(\sigma^g f_b^g - \frac{\lambda^m}{\lambda^g - \lambda^m} \eta_i \sigma^m f_b^m \right) \Phi N_0 \epsilon_\gamma I_\gamma \frac{t_{live}}{t_m} K_\gamma f_w f_c C_{sum},$$

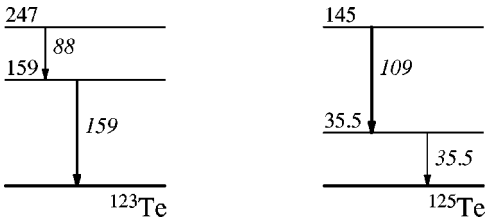

FIG. 7. Simplified decay scheme of $^{123}Te^m$ and $^{125}Te^m$. All energies are given in units of keV. The transitions used for analysis are indicated by thick arrows.

$$b := \frac{\lambda^m}{\lambda^g - \lambda^m} \eta_i \sigma^m f_b^m \Phi N_0 \epsilon_\gamma I_\gamma \frac{t_{live}}{t_m} K_\gamma f_w f_c C_{sum},$$

where $\sigma^{g,m}$ denotes the partial capture cross section to the ground, and isomeric state, respectively, Φ the time integrated neutron flux, N_0 the total number of nuclei of the respective isotope in the Te sample, ϵ_γ the efficiency of the clover detector for the geometry used, I_γ the relative intensity for the γ line used for identification of the ground state decay, and t_{live}/t_m the dead time correction. K_γ accounts for the correction for γ-ray self-absorption in the sample. The time factors $f_w = e^{-\lambda t_w}$ and $f_c = (1 - e^{-\lambda t_m})$ account for the fraction of nuclei that decay during the waiting time between irradiation and measurement and during the γ-ray counting itself, C_{sum} for the summing correction. Pile-up corrections could be neglected.

Since a and b are determined by fitting the activity of one γ line, the ratio does not depend on most of the correction factors:

$$\nu := a/b = \frac{\sigma^g f_b^g}{\eta_i \sigma^m f_b^m} \frac{\lambda^g - \lambda^m}{\lambda^m} - 1,$$

hence

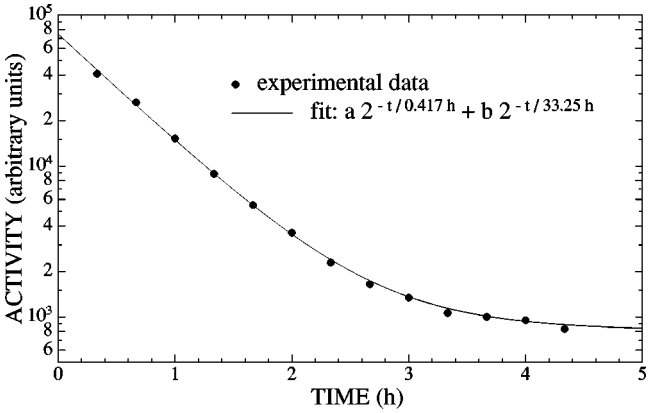

FIG. 8. Time dependence of the decay $^{131}Te^g$ after the reactor activation illustrated by the intensity of the 150-keV transition in ^{131}I. Each point represents a measuring time of 20 min. The solid curve corresponds to the sum of two independent least square fits with exponentials corresponding to the half-lives of ground and isomeric state.

TABLE II. Decay parameters used for analysis from Ref. [6].

Isotope	Half-life time	Internal decay	γ energy (keV)	Line intensity
$^{123}Te^m$	119.7±0.1 d	1	159	0.8404
$^{127}Te^m$, $^{127}Te^g$	109±2 d; 9.35±0.07 h	0.976±0.002	417.9	0.0099
$^{129}Te^m$, $^{129}Te^g$	33.6±0.1 d; 1.160±0.003 h	0.65±0.03[a]	459.6	0.0737±0.0024
$^{131}Te^m$, $^{131}Te^g$	33.25±0.25* h; 25.0±0.1 min	0.259±0.005[a]	149.7	0.689±0.0006

[a]Adopted from this work (see Sec. III D).

$$\frac{\sigma^m}{\sigma^g}=\frac{1}{\nu+1}\frac{\lambda^g-\lambda^m}{\lambda^m}\frac{f_b^g}{\eta_i f_b^m},$$

$$\frac{\sigma^m}{\sigma^g+\sigma^m}=\frac{(\lambda^g-\lambda^m)f_b^g}{(\nu+1)\lambda^m\eta_i f_b^m+(\lambda^g-\lambda^m)f_b^g}.$$

The remaining sources of uncertainties are due to the adopted decay data, in particular related to the half-lives and the internal decay of the isomer, to the time corrections, and to counting statistics. The resulting systematic and statistical uncertainties are given in Table III together with the isomeric ratios. Except for $^{126}Te(n,\gamma)$, the total uncertainties are always dominated by the systematic component.

The isomeric ratios are compared in Table III with previously reported data. This comparison is somewhat hampered by the fact that the present experiment did not distinguish between thermal and epithermal neutrons. This should not cause a significant effect, however, since (i) the thermal and epithermal values given in Ref. [4] are very similar, and (ii) the epithermal component in the present activations was rather small according to the measured flux ratio of (5.5 ±0.5)%. Given the discrepancies between Refs. [4] and [5] the results reported here are in agreement with Ref. [5] for ^{126}Te whereas they clearly support the values for ^{128}Te given in Ref. [4]. For ^{130}Te the sizable uncertainties of previous data [5] could be considerably reduced.

Nevertheless, this comparison shows that the thermal Te cross sections need further improvement. While the present experiment was aiming at cross section ratios, these results are indicating yet unsolved problems with the total capture cross sections.

D. Other nuclear data

Apart from the isomeric ratios it was also possible to determine some decay data of the long-lived tellurium isomers with improved accuracy. Accordingly, these values were used in the present analysis.

While the half-life of $^{131}Te^m$ was reported as 30±2 h [6] a least square fit to the present data for the 150-keV γ line shown in Fig. 9 yields

$$t_{1/2}(^{131}Te^m)=33.25\pm0.25\ \text{h}.$$

The half-lives of all other investigated nuclei were known before with uncertainties of less than 1%.

For $^{129}Te^m$ the fraction of internal decays could be determined by comparing the intensities of the 459.6-keV γ line from the ground state decay with the 695.88-keV γ line of the isomer decay at late times. With the respective decay intensities of 0.03 059±0.00 096 (for the 695.88-keV line) and 0.0736±0.0024 (for the 459.6-keV line) [6] one finds

$$\eta_i(^{129}Te)=0.649\pm0.030,$$

in very good agreement with, but more accurate than the value of 0.65±0.06 given in Ref. [6].

A similar analysis was possible for the decay of $^{131}Te^m$ via the γ lines at 149.7 keV for the ground state ($I_\gamma=0.689\pm0.006$) and 200.6 keV for the isomer ($I_\gamma=0.07\,546\pm0.00\,116$). Since (5.07±0.66)% of the isomeric decays emit also a 149.7-keV γ ray, one obtains

$$\eta_i(^{131}Te)=0.2594\pm0.0054.$$

Within two standard deviations, this result is compatible with the previous value of 0.222±0.016 reported in Ref. [6].

IV. ANALYSIS OF THE VAN DE GRAAFF ACTIVATION

A. Determination of the neutron flux

The induced ^{198}Au activity was determined via the net counts, in the 412-keV line of the ^{198}Au decay measured with the 40-cm^3 HPGe detector,

TABLE III. Isomeric ratios measured in the reactor activation in comparison to previous data.

Reaction	Thermal [4]	Epithermal [4]	Thermal [5]	Thermal+epithermal (this work)[a]
$^{126}Te(n,\gamma)^{127}Te^{m,g}$	0.06±0.01	0.0796±0.0079	0.13±0.03	0.149±0.004 (1.4/2.0)
$^{128}Te(n,\gamma)^{129}Te^{m,g}$	0.127±0.01	0.125±0.009	0.070±0.005	0.124±0.008 (2.2/6.2)
$^{130}Te(n,\gamma)^{131}Te^{m,g}$			0.07±0.04	0.067±0.005 (3.2/7.3)

[a]Values in brackets are the statistical and systematic uncertainties in %, respectively.

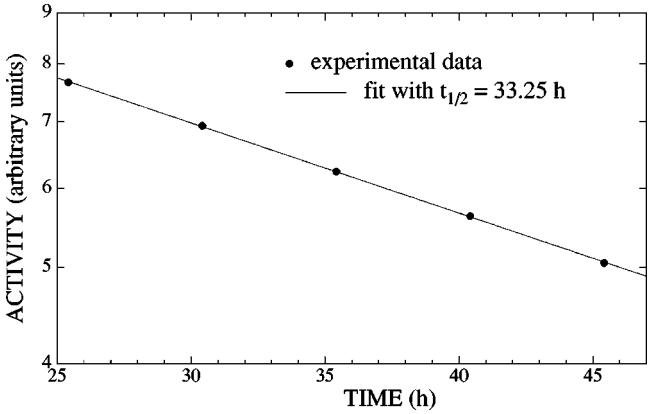

FIG. 9. Same decay as shown in Fig. 8 but for later times when the ground state contribution was completely negligible. Each point represents a measuring time of 5 h. The solid curve corresponds to a least square fit for determining the improved half-life.

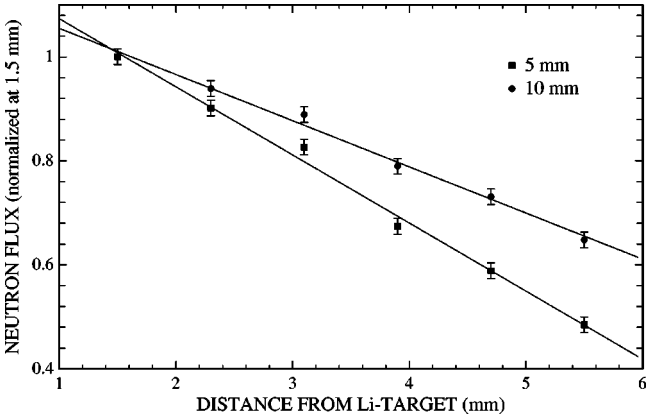

FIG. 10. The neutron flux versus distance between neutron target (6-mm diameter) and sample, measured by irradiation of a stack of gold foils. The linear dependence is confirmed for gold foils of 5- and 10-mm diameter.

$$C_\gamma = N\,\epsilon_\gamma I_\gamma \frac{t_{live}}{t_m} K_\gamma f_w f_m ,$$

where N denotes the total number of activated nuclei at the end of irradiation, $\epsilon_\gamma = (1.99 \pm 0.04) \times 10^{-5}$ the efficiency of the Ge detector for the geometry used [13], $I_\gamma = 0.9558 \pm 0.0012$ the relative intensity for the 412-keV line [14], and t_{live}/t_m the dead time correction. K_γ, the correction for γ-ray self absorption in the 30-μm-thick gold foils, could be neglected. The time factors $f_w = e^{-\lambda t_w}$ and $f_m = (1 - e^{-\lambda t_m})$ account for the fraction of nuclei that decay during the waiting time between irradiation and measurement and during the measurement itself, and are discussed elsewhere [7]; λ is the decay constant of the respective product nucleus. Pile-up and summing corrections could be neglected in this measurement due to the 76-mm distance between sample and detector, and the comparably small detector efficiency.

The total number of activated nuclei, ^{198}N, is given by

$$^{198}N = \Phi_{tot}^{197} N\, \sigma_{\mathrm{Au}} f_b ,$$

where $\Phi_{tot} = \int \Phi(t)\, dt$ is the time–integrated neutron flux, ^{197}N the number of gold atoms, and $\sigma_{\mathrm{Au}} = 648 \pm 10$ mb [8] the spectrum-averaged neutron capture cross section. The time factor f_b corrects for the decay during activation, including the effects due to a time variation of the neutron flux (for a definition see Ref. [7]). Since the neutron flux is determined by the gold foils on both sides of the sample, corrections for target geometry as well as for neutron scattering and self-shielding are accounted for by averaging the neutron fluxes obtained from the two gold foils.

The total flux uncertainty was determined by quadratic summation of the various systematic errors, since the influence of the counting statistics in measuring the activity of the gold foils was negligible. Apart from the above effects, a 7% uncertainty was allowed to account for the flux at the position of the Te samples. This corresponds to a 0.5-mm uncertainty in the position of the sample relative to the gold foils according to the linear decrease of the induced activity with the distance from the neutron target as measured by activation of a stack of five gold foils (Fig. 10). The uncertainty in determining the mass of the gold foils was negligibly small. The information on sample mass and various run parameters are summarized in Table IV.

B. Induced activities

With the method described in the previous section the isomeric ratios have also been measured in the keV neutron energy range, thus reducing the systematic uncertainties significantly. Though also the total capture cross section could have been determined, the main focus of this experiment was on the possible branchings caused by the yet unknown partial cross sections populating the long-lived isomers in ^{127}Te and ^{131}Te, which were unknown so far.

After the first activation of 1.5 h the activity was counted for 18 h with the Clover system. The spectra have been saved every hour for determining the time dependence of the activity. From these data the ^{130}Te(n,γ) cross section information were derived. The second activation lasted 3 d and the produced activity was counted for 16 d, again with the Clover system. The spectra were saved every hour immediately after the activation and every 4 h at later times.

The analysis of the recorded spectra was performed as described for the reactor activations, using the different time constants to separate the decays of the various isotopes.

TABLE IV. Parameters of the activations at the Van de Graaff accelerator).

Sample	Mass (mg)	Irradiation time (h)	Integral flux (cm^{-2})	Uncertainty (%)
TE1	105	1.48	1.03×10^{13}	3.2
TE2	126	68.25	1.99×10^{14}	3.0

TABLE V. Isomeric ratios for a stellar neutron spectrum corresponding to $kT=25$-keV thermal energy.

Reaction	Ref. [15]	This work[a]
^{126}Te$(n,\gamma)^{127}$Te^{m,g}		0.342±0.027 (0.8/8.0)
^{128}Te$(n,\gamma)^{129}$Te^{m,g}	0.111±0.006	0.070±0.017 (0.3/24.8)
^{130}Te$(n,\gamma)^{131}$Te^{m,g}		0.269±0.022 (0.8/8.3)

[a]Values in brackets are the statistical and systematic uncertainties in %, respectively.

C. Results and uncertainties

The resulting isomerc ratios are listed in Table V, which also includes the only previous experimental value for comparison. As far as the total capture cross sections of ^{126,128,130}Te are concerned, the values derived from the present data agree with previous experiments, but exhibit larger uncertainties since the activation times at the Van de Graaff accelerator were optimized for the isomers in ^{126}Te and ^{130}Te. For this reason, the isomeric ratio of ^{128}Te exhibits a comparably large systematic uncertainty.

Because of the high detection efficiency of the Clover system, the statistical uncertainties are below 1% for all three cases listed in Table V. In addition to the uncertainties of the nuclear data used (Table II), the f_b factor, which accounts for the number of decays already during the activation, adds significantly to the systematic uncertainties. Since the flux at the Van de Graaff accelerator is not constant in time, mainly due to the degradation of the Li target, f_b needs to be determined numerically. The shorter the half-life of the produced isotope compared to the irradiation time, the larger the uncertainty of f_b. This holds in particular for ^{128}Te, where the isomeric ratio required a three day activation, whereas the half-life of the ground state is only 70 min. In this case the 23% uncertainty of the f_b correction completely dominates the systematic uncertainty.

Comparison of the isomeric ratios at thermal energies and in the keV region shows surprisingly large effects. Obviously, the partial cross sections feeding the isomers in ^{127}Te and ^{131}Te are enhanced at keV energies, a trend which may be due to the larger number of initial states. On the other hand, the partial cross section to the isomer in ^{129}Te shows no such enhancement, in spite of the close similarity in the nuclear structure of the final states.

V. SUMMARY AND ASTROPHYSICAL IMPLICATIONS

The activation at thermal energy has produced results in two areas. In addition to the intended improvement of the isomeric ratios of the four isotopes^{120}Te, ^{126}Te, ^{128}Te, and^{130}Te, the accuracy of some decay data, i.e., the half-life of ^{131}Te^m and the IT decay branchings of ^{129}Te^m and ^{131}Te^m, could be improved as well.

In the activations in the quasi-stellar neutron spectrum for $kT=25$ keV, first experimental values for the isomeric ratios of ^{126}Te and ^{130}Te could be obtained. In all relevant cases, overall uncertainties of 8% could be obtained.

Among these results, the isomeric ratio of ^{126}Te was important for estimating the impact on the branching in the *s*-process reaction chain at ^{127}Te, in particular since this IR—and hence the population of the 109-d isomer—is more than two times larger at stellar temperatures than suggested by the thermal value. So far, astrophysical models assumed that this isomer is quickly depopulated to the short-lived ground state by thermally induced transitions to higher lying excited states with a decay branch to the ground state. With this assumption and with the previously adopted thermal value of the IR the effective half-life of^{127}Te is sufficiently short to reduce this branching to a negligible level. With the larger stellar value of the IR obtained in this work, however, the question has to be addressed again, whether the 109-d isomer is indeed quickly destroyed by thermally induced transitions. For example, if it turns out that it may survive at the lower temperature of $T_8=1$, where the AGB stars produce 95% of their neutrons, the^{127}Te branching could be as large as 10% and could no longer be neglected in the interpretation of the main branching at ^{128}I.

ACKNOWLEDGMENTS

We are grateful for the support during the activations at the reactor in Heidelberg by Mr. and Mrs. Jünger as well as at the Karlsruhe Van de Graaff accelerator by E.-P. Knaetsch, D. Roller, and W. Seith. Our thanks also go to A. Mengoni and R. Gallino for many discussions concerning the physics and astrophysics issues of this work. One of us (R.R.) would like to thank CERN for financial support.

[1] R. Gallino, M. Busso, and M. Lugaro, in *Astrophysical Implications of the Laboratory Study of Presolar Material*, edited by T. Bernatowitz and E. Zinner (AIP, Woodbury, NY, 1997), p. 115.
[2] R. Gallino, C. Arlandini, M. Busso, M. Lugaro, C. Travaglio, O. Straniero, A. Chieffi, and M. Limongi, Astrophys. J. **497**, 388 (1998).
[3] K. Takahashi and K. Yokoi, At. Data Nucl. Data Tables **36**, 375 (1987).
[4] V. Alpatov, A. Davydov, G. Kartashov, M. Korotkow, G. Kostina, P. Polozov, and A. Sadovskii, At. Data Nucl. Data Tables **58**, 13 (1995).
[5] J. Mughabghab, M. Divadeenam, and N. Holden, *Neutron Cross Sections* (Academic, New York, 1981), Vol. 1, Part A.
[6] C. Nordborg, H. Gruppelaar, and M. Salvatores, in *Nuclear Data for Science and Technology*, edited by S. Qaim (Springer, Berlin, 1992), p. 782.
[7] H. Beer and F. Käppeler, Phys. Rev. C **21**, 534 (1980).
[8] W. Ratynski and F. Käppeler, Phys. Rev. C **37**, 595 (1988).
[9] R. Auble, Nucl. Data Sheets **40**, 301 (1983).

[10] S. Jaag, technical report, Forschungszentrum Karlsruhe, 1993.
[11] S. Abramovich *et al.*, technical report, CERN, Geneva, Switzerland, 1999, report CERN/SPSC 99-8; SPSC/P 310.
[12] S. Jaag and F. Käppeler, Phys. Rev. C **51**, 3465 (1995).
[13] M. Schumann (private communication).
[14] Z. Chunmei, Nucl. Data Sheets **74**, 259 (1995).
[15] Z. Bao, H. Beer, F. Käppeler, F. Voss, K. Wisshak, and T. Rauscher, At. Data Nucl. Data Tables **76**, 70 (2000).